Synchronization Errors and SINR Performance: How Critical Are They in Cell-Free Massive MIMO with Ultra-Dense LEO Satellite Connectivity?

Reza Mahin Zaeem, Juan Carlos Merlano Duncan, Vu Nguyen Ha, Symeon Chatzinotas, and Björn Ottersten
Interdisciplinary Centre for Security, Reliability, and Trust (SnT), Universite du Luxembourg, Luxembourg, Luxembourg
Emails: {reza.zaeem, juan.duncan, vu-nguyen.ha, symeon.chatzinotas, bjorn.ottersten}@uni.lu

2024 IEEE 99th Vehicular Technology Conference (VTC2024-Spring) | 979-8-3503-8741-4/24/$31.00 ©2024 IEEE | DOI: 10.1109/VTC2024-SPRING62846.2024.10683325

***Abstract*—This paper delves into the dynamics of resource allocation in ultra-dense Low Earth Orbit (LEO) satellite networks within a cell-free massive MIMO framework, focusing on the impact of residual synchronization errors. We conduct various analyses to understand how these errors – encompassing time, phase, and frequency – influence the Signal-to-Interference-plus-Noise Ratio (SINR) and the average number of satellite links connected to each user. Our approach measures the effects of these remaining synchronization errors and uses these values to inform and optimize power and resource allocation decisions. The study reveals that as synchronization errors increase, the number of effective satellite links to users diminishes, consequently reducing the number of satellites actively connected to each user. This research not only highlights the critical impact of synchronization errors on network performance but also demonstrates how advanced knowledge of these error variances can significantly enhance resource allocation strategies and network efficiency in future ultra-dense LEO satellite systems.**

I. Introduction

The profound significance of Cell-Free (CF) Massive MIMO (mMIMO) in ultra-dense LEO satellite networks (UD-LEONs) is set to transform global connectivity and service quality [1]–[3]. Enabling multiple antennas cooperatively serving all users simultaneously, CF mMIMO enhances spectral efficiency and network flexibility, crucial for the vast coverage requirements of LEO networks [4]. This system is particularly crucial in space, addressing user density and demand variations, and overcoming traditional cellular limitations like cell boundary perception and interference [5], [6]. Its role in ensuring coherent operation and mitigating time alignment errors is essential for consistent service quality in the dynamic environment of UD-LEONs [1], [4].

Synchronization is crucial for distributed systems, especially in UD-LEONs and CF mMIMO systems [7], [8]. Precise alignment of phases and clocks is essential for coherent operation, and discrepancies in time, phase, and frequency can significantly degrade performance [9], [10]. Asynchronous receptions, common in distributed MIMO systems due to signal propagation delays and hardware inaccuracies, introduce phase shift matrices to the estimated CSI, lowering spectral efficiency and signal quality [11], [12]. This desynchronization leads to severe multi-user interference, pilot orthogonality destruction, Inter-Symbol Interference (ISI), and signal phase misalignment, all of which undermine the constructive signal combination crucial for effective precoding and detection [13].

Time, phase, and frequency synchronization errors in UD-LEONs and CF mMIMO systems stem from various sources, each impacting system performance and reliability [1], [14]. Imperfect estimations of relative positions and velocities of nodes, oscillator instabilities, and environmental factors like multipath and atmospheric conditions are significant contributors [10], [15]. In LEO systems, satellites' high mobility relative to ground terminals introduces Doppler shifts affecting frequency synchronization, while propagation delays over vast distances lead to time synchronization issues [7], [8]. Additionally, low-cost oscillators and inherent hardware imperfections cause phase and frequency errors [16]. These synchronization errors are further pronounced with increasing SNR, the number of antennas per satellite, and the subcarrier sequence number [4], [15]. Addressing these synchronization errors is essential to maintain high data rates, spectral efficiency, and consistent service quality in the UD-LEONs [13].

In CF Massive MIMO and LEO satellite systems, a critical research gap lies in addressing the impact of non-negligible synchronization errors on SINR and network efficiency [7], [8], [10]. Our study addresses this by investigating how residual time, phase, and frequency synchronization errors influence SINR and the implications for power and resource allocation. We introduce a novel approach that integrates these errors into the allocation framework, enhancing resource distribution in LEO networks. Additionally, we explore the impact of these errors on the number of user-satellite connections, a crucial factor for network performance. Our research contributes significantly to understanding and mitigating synchronization challenges, thereby improving the service quality and efficiency of ultra-dense LEO systems.

II. System Model

We consider a CF Massive MIMO system employing LEO satellites, referred to as Satellite Access Points (SAPs), and a set of User Equipments (UEs). The system comprises M SAPs and K UEs, where each UE is equipped with a single antenna, and each SAP has N antennas. The SAPs are organized into clusters, each connected to a Central Processing Unit (CPU) located on a Super Satellite Node (SSN) for advanced computational capabilities. The communication between SAPs and the CPU is facilitated through high-speed Inter-Satellite Links (ISLs), e.g. Free-Space Optical communications [4].

A. TDD-based Satellite Communications

The data communication between SAPs and UEs is operated based on a Time-Division Duplex (TDD) protocol

979-8-3503-8741-4/24/$31.00 ©2024 IEEE
Authorized licensed use limited to: Univ of Science and Tech Beijing. Downloaded on February 19,2025 at 04:30:09 UTC from IEEE Xplore. Restrictions apply.

leveraging the channel reciprocity between uplink (UL) and downlink (DL). In particular, a regarded coherence time slot of τ_c (seconds) is assumed to contain three segments:

(a) UL pilot transmission with a duration of τ_{p}.
(b) UL data transmission with a duration of $\tau_{\mathsf{dt}}^{\mathsf{ul}}$.
(c) DL data transmission with a duration of $\tau_{\mathsf{dt}}^{\mathsf{dl}}$.

Note that guard intervals are considered outside this coherence time. The UL pilots are utilized for channel estimation at the SAPs, supporting the scalability of the network and reducing signaling overhead. These channel estimates are subsequently used for DL data precoding and UL data detection.

1) Channel Model: In our analysis, we adopt a channel model similar to that presented in [4]. Specifically, the channel between SAP m and UE k is modeled as

$$\boldsymbol{h}_{mk} = \sqrt{\beta_{mk}} + \sqrt{\lambda_{mk}}\boldsymbol{h}'_{mk}, \tag{1}$$

where $\boldsymbol{h}'_{mk} \sim \mathcal{CN}(0,1)$ represents the small-scale fading component. The parameters β_{mk} and λ_{mk} correspond to the line-of-sight (LoS) and non-line-of-sight (NLoS) components, respectively, which are calculated as $\sqrt{L_{mk}\frac{\kappa_{mk}}{\kappa_{mk}+1}}$ and $\sqrt{L_{mk}\frac{1}{\kappa_{mk}+1}}$ where κ_{mk} is the Rician K-factor. Herein, L_{mk} denotes the large-scale fading factor, which includes path loss, shadowing, and antenna gains as detailed in [4], [19], [20].

B. Uplink Training and Channel Estimation

In the UL transmission, the UEs transmit pilot signals during the initial phase with T_{p} samples of the coherence block. These samples are then utilized for the channel estimation at the SAPs. Given $K > T_{\mathsf{p}}$, some UEs have to share the same pilot sequence (PS). Let introduce binary variable $a_{k,k'}$ as

$$a_{k,k'} = \begin{cases} 1, & \text{if UEs } k \text{ and } k' \text{ assigned the same PS,} \\ 0, & \text{otherwise.} \end{cases} \tag{2}$$

Then, the set of UEs assigned the same PS as UE k can be denoted as

$$\Psi_k = \{k' | a_{k,k'} = 1\}. \tag{3}$$

Denote $\boldsymbol{\phi}_k \in \boldsymbol{C}^{T_{\mathsf{p}}}$ the PS assigned to UE k and all UE $k' \in \Psi_k$). One assume that $\boldsymbol{\phi}_k$ is transmitted with power p_k. Then, the received signal at SAP m can be described as

$$\boldsymbol{r}_m^{\mathsf{p}} = \sum_{k=1}^{K} \sqrt{p_k}\boldsymbol{h}_{mk}\boldsymbol{\phi}_k + \boldsymbol{n}_m, \tag{4}$$

where $\boldsymbol{n}_m \sim \mathcal{CN}(0, \sigma^2 I_{T_{\mathsf{p}}})$ is the AWGN vector, and $I_{T_{\mathsf{p}}}$ is $T_{\mathsf{p}} \times T_{\mathsf{p}}$ identity matrix. Then, the UL channel corresponding to UE k at SAP m can be estimated as

$$\hat{r}_{mk}^{\mathsf{p}} = \boldsymbol{\phi}_k^H \boldsymbol{r}_m^{\mathsf{p}} = \sqrt{p_k}T_{\mathsf{p}}\boldsymbol{h}_{mk} + \sum_{k' \in \Psi_k \setminus \{k\}} \sqrt{p_{k'}}T_{\mathsf{p}}\boldsymbol{h}_{mk'} + \boldsymbol{\phi}_k^H n_m. \tag{5}$$

We assume perfect synchronization in the UL phase. This assumption simplifies the estimation but may not reflect all real-world conditions. The estimated channel vector between SAP m and UE k obtained by using the Linear Minimum Mean Square Error (LMMSE) method [18] is given as

$$\hat{\boldsymbol{h}}_{mk} = \left(\sqrt{p_k}\lambda'_{mk}/\beta'_{mk}\right)\boldsymbol{\phi}_k^H \boldsymbol{r}_m, \tag{6}$$

where $\lambda'_{mk} = \lambda_{mk} + \beta_{mk}$ and $\beta'_{mk} = \sum_{l \in \psi_k} T_{\mathsf{p}}\hat{p}_l\lambda'_{ml} + \sigma_w^2$.

***Remark** 1:* Here, it is worth noting that the expected value of the LMMSE estimate $\hat{\boldsymbol{h}}_{mk}$ is zero, and its variance is given by $\frac{\hat{p}_k T_{\mathsf{p}}(\lambda'_{mk})^2}{\beta'_{mk}}$. Similarly, the expected value of the estimation error $\tilde{\boldsymbol{h}}_{mk}^{\mathsf{lmmse}}$ is zero, with its variance of $\lambda'_{mk} - \frac{\hat{p}_k(\lambda'_{mk})^2}{\beta'_{mk}}$.

C. Downlink Data Transmission

For DL transmission, we first present SAP-UE association variables, γ_{mk}'s, where

$$\gamma_{mk} = \begin{cases} 1, & \text{if SAP } m \text{ is assigned to serve UE } k, \\ 0, & \text{otherwise.} \end{cases} \tag{7}$$

Similar to [9]–[12], the received signal at UE k during the downlink transmission phase can be modeled as

$$\boldsymbol{y}_k(t) = \sum_{m=1}^{M} \boldsymbol{h}_{mk}^H \boldsymbol{x}_m(t - \delta_{mk}^{\mathsf{T}}) e^{j2\pi[(t-\delta_{mk}^{\mathsf{T}})(f-\delta_{mk}^{\mathsf{F}})+\delta_{mk}^{\mathsf{P}}]} + n_k(t), \tag{8}$$

where $\boldsymbol{x}_m(t) = \sum_{k=1}^{K} \sqrt{\gamma_{mk}\eta_{mk}}\boldsymbol{w}_{mk}q_k(t)$ is the precoded signal transmitted by SAP m; $\boldsymbol{w}_{mk} \in \boldsymbol{C}^N$ is the precoding vector corresponding to UE k at SAP m with $E\{\|\boldsymbol{w}_{mk}\|^2\} = 1$; η_{mk} is the normalized transmit power, satisfying a per-AP power constraint; δ_{mk}^{T}, δ_{mk}^{F}, and δ_{mk}^{P} represent the time, frequency, and phase mis-synchronization errors, respectively; $n_k(t)$ represents the noise at UE k, $n_k \sim \mathcal{CN}(0,1)$. It is worth noting that signal processing task, including data precoding and power control, is jointly performed at the SSN. Furthermore, all required information for signal processing tasks is collected through the ISLs. In addition, the relation between γ_{mk} and η_{mk} can presented as [21], [22]

$$\gamma_{mk} = \|\eta_{mk}\|_0, \quad \forall(m,k), \tag{9}$$

where $\|*\|_0$ stands for the norm-ℓ_0.

***Remark** 2:* In the DL transmission, time-synchronization errors can lead to a shift in the transmitted symbols, causing them to spill over into adjacent time slots. This results in the misalignment between the transmitted and received symbols. To quantify this effect, we assume that a fraction of $\sqrt{1-\alpha_{mk}}$ for ISI. This assumption can be strengthened based on that η_{mk}'s and $\boldsymbol{w}_{mk}$'s remain constant for each coherence time, which allows us to isolate the effect of timing errors.

Thanks to Remark 2, the received signal at each sampling instance during the DL transmission, reflecting the impact of synchronization errors, can be expressed as follows

$$\boldsymbol{y_k} = \sum_{m=1}^{M}\sum_{k=1}^{K} \Big(\boldsymbol{h}_{mk}^H \boldsymbol{w}_{mk} \sqrt{\gamma_{mk}\eta_{mk}\alpha_{mk}}\; e^{j2\pi[\delta_{mk}^{\mathsf{F}}+\delta_{mk}^{\mathsf{P}}]} q_k + \boldsymbol{h}_{mk}^H \boldsymbol{w}_{mk} \sqrt{\gamma_{mk}\eta_{mk}} \sqrt{1-\alpha_{mk}} q'_k \Big) + n_k, \tag{10}$$

Here, the time index is omitted for simplicity. In (10), q'_k represents the summation of several symbols intended to be received by user k'. Hence, q_k and q'_k are independent and identically distributed with zero mean and unit variance. The phenomenon of symbol spill-over, represented by q'_k, can be attributed to the influence of Doppler shift-induced time synchronization errors. Doppler shift introduces timing discrepancies, which cause a portion of each symbol q_k to extend into neighboring time slots, effectively manifesting as interference in the received signal. We also assume that $\delta_{mk}^{\mathsf{T}}\delta_{mk}^{\mathsf{F}}$ in (10) are negligible compared to δ_{mk}^{T} and δ_{mk}^{F}.

Authorized licensed use limited to: Univ of Science and Tech Beijing. Downloaded on February 19,2025 at 04:30:09 UTC from IEEE Xplore. Restrictions apply.

D. Measurement of the Expected Value of SINR

Regarding the data transmission over the downlink, accurately measuring the SINR for each user is crucial for assessing system performance and quality of service. By analyzing the received signal as defined previously, we can extract the necessary components to calculate the SINR for each user. $y_k = G_k^{CP} q_k + I_k^{PU} q_k + I_k^T q_k + \sum_{k' \neq k} I_{kk'}^U$.

$$SINR_k = \frac{|G_k^{CP}|^2}{|I_k^T|^2 + E\{|I_k^{PU}|^2\} + \sum\limits_{k' \neq k} E\{|I_{kk'}^U|^2\} + 1}. \quad (11)$$

In (11), $G_k^{CP} = \sum_{m=1}^{M} \sqrt{\gamma_{mk}\eta'_{mk}} E\{\boldsymbol{h}_{mk}^H \boldsymbol{w}_{mk} e^{j2\pi[\delta_{mk}^{\mathsf{F}} + \delta_{mk}^{\mathsf{P}}]}\}$ represents the coherent gain from the desired signal, aggregating the channel gains across all satellites. $I_k^{PU} = \sum_{m=1}^{M} \sqrt{\gamma_{mk}\eta'_{mk}} (\boldsymbol{h}_{mk}^H \boldsymbol{w}_{mk} - E\{\boldsymbol{h}_{mk}^H \boldsymbol{w}_{mk}\})$ captures the power uncertainty interference from channel estimation variations. $I_{kk'}^U = \sum_{m=1}^{M} \sqrt{\gamma_{mk}\eta'_{mk'}} \boldsymbol{h}_{mk}^H \boldsymbol{w}_{mk'} e^{j2\pi[\delta_{mk}^{\mathsf{F}} + \delta_{mk}^{\mathsf{P}}]}$ accounts for ISI, and $I_k^T = \sum_{m=1}^{M} \sqrt{\gamma_{mk}\eta''_{mk}} E\{\boldsymbol{h}_{mk}^H \boldsymbol{w}_{mk} e^{j2\pi[\delta_{mk}^{\mathsf{F}} + \delta_{mk}^{\mathsf{P}}]}\}$ represents the interference from time synchronization errors. The power allocation coefficients, $\eta'_{mk} = \eta_{mk}\alpha_{mk}$ and $\eta''_{mk} = \eta_{mk}(1 - \alpha_{mk})$, are adjusted for resource allocation and synchronization error considerations. Together, these components provide a comprehensive understanding of SINR experienced by users, considering various signal and interference sources in satellite communications.

E. Problem Formulation

In this work, we aim to maximize the minimum rate of all K users in the system while taking into account resource allocation (γ_{mk} and η_{mk}), pilot assignment (Ψ_k), and synchronization errors (δ_{mk}^{T}, δ_{mk}^{P}, δ_{mk}^{F}). Here, the user rates can be recast by the expected value of SINRs, i.e., $SINR_k(\gamma_{mk}, \eta_{mk}, \Psi_k, \delta_{mk}^{\mathsf{T}}, \delta_{mk}^{\mathsf{P}}, \delta_{mk}^{\mathsf{F}})$, which are the functions of the power allocation, resource allocation, pilot assignment, synchronization errors in time, phase, and frequency. The problem can be written as

$$(\mathcal{P}_1): \max_{\gamma_{mk}, \eta_{mk}, \Psi_k} \min_k \; SINR_k(\gamma_{mk}, \eta_{mk}, \Psi_k, \delta_{mk}^{\mathsf{T}}, \delta_{mk}^{\mathsf{P}}, \delta_{mk}^{\mathsf{F}})$$

$$\textbf{s. t.} \quad \text{(C1)}: \quad \sum_{k=1}^{K} \gamma_{mk}\eta_{mk} \leq P_m^{\max}, \quad \forall m, \quad (12a)$$

$$\text{(C2)}: \quad \min_k R_k > r_0, \quad \forall k, \quad (12b)$$

$$\text{(C3)}: \quad \gamma_{mk} \in \{0, 1\}, \quad \forall m, k, \quad (12c)$$

$$\text{(C4)}: \quad 1 \leq |\Psi_k| \leq U, \quad \forall k. \quad (12d)$$

In (12), constraint (C1) is considered to ensure that each SAP's maximum transmission power $P_m^{\max}$ is not violated, while (C2) implies the quality of service requirement at every UE. Additionally, (C3) pertains binary requirement given in (7), while (C4) addresses pilot assignment, ensuring that the number of users sharing the same pilot sequence remains within the bounds set by U, thus balancing pilot reuse and minimizing pilot contamination.

The synchronization errors in the network, characterized by their variances, are crucial parameters in our study. The variances of these synchronization errors, computed as per methodologies outlined in [9], [10], play a pivotal role in the decision-making process for resource allocation. The SSNs, central to our network's architecture, possess knowledge of these synchronization error variances and can share this information with other SAPs in their clusters. This information is instrumental in optimizing the power allocation and resource scheduling strategies across the network.

III. Proposed Solution Approach

Delving into various aspects crucial for the performance of the Cell-Free Massive MIMO system with LEO satellites, this section discusses a simple approach to address $(\mathcal{P}_1)$. It encompasses a detailed examination of resource allocation strategies, power control mechanisms, precoding schemes, and the overall solution to the optimization problem. The primary focus is to enhance the system's efficiency and reliability while maintaining robust communication between satellites and ground users. Each of the following subsections will address specific components and their roles in optimizing performance.

A. SAP Association Solution

For simplicity, we propose to select γ_{mk} based solely on the large-scale fading parameters from each SAP regarding both LOS and NLOS components. In particular, each SAP utilizes the LMMSE channel estimator to make local association decisions according to a threshold percentage ν. An approach similar to that detailed in [23] has been employed at every SAP (i.e., SAP m), as follows.

(a) If the sum of the most substantial channel gains from SAP m to its UEs exceeds $\nu\%$, we set $\gamma_{mk} = 1$ for those users, indicating they are served by this SAP.
(b) For the rest, $\gamma_{mk} = 0$. By increasing this parameter to 1, we enable SAP m to communicate with the k^{th} user.
(c) In the final stage, if the power coefficient η_{mk} tends to zero, we consider that link as having no communication, thus setting $\gamma_{mk} = 0$.

B. Precoding Design

In this CF mMIMO system, we aim to employ Maximum Ratio Transmission (MRT) precoding for its simplicity and direct approach to enhancing signal strength at the receiver. The MRT is particularly appealing for its straightforward implementation and effective utilization of channel state information. Specifically, the precoding vector applied to the data transmission of UE k at SAP m can be given as

$$\boldsymbol{w}_{mk} = \hat{\boldsymbol{h}}_{mk} / \|\hat{\boldsymbol{h}}_{mk}\|, \quad (13)$$

where $\hat{\boldsymbol{h}}_{mk}$ represents the estimated channel vector between SAP m and UE k. This choice allows for an uncomplicated yet insightful analysis of the satellite communication system's performance, focusing on the impact of resource allocation and synchronization errors without delving into the complexities of more advanced precoding techniques.

Authorized licensed use limited to: Univ of Science and Tech Beijing. Downloaded on February 19,2025 at 04:30:09 UTC from IEEE Xplore. Restrictions apply.

C. Pilot Assignment Solution

While the primary objective of this paper is to maximize the system performance through optimal pilot sequences and pilot assignment, achieving scalability in this process is crucial. To address this challenge, we adopt an effective pilot-assignment methodology similar to the one utilized in [23], where UEs are assigned the pilot signals based on their geographical locations. This approach is not only scalable but also allows each SAP to gain a priori knowledge about how to categorize each UE and subsequently determine the sets Ψ_k. Under this scheme, SAPs use geographical information to effectively assign pilot sequences, and as a result, U can be bounded by $\lceil K/T_{\mathsf{p}} \rceil$.

D. Problem Solution

After simplifying the SAP association, precoding design, and pilot assignment tasks as outlined in the previous subsections, the original problem $(\mathcal{P}_1)$ can be relaxed where the remaining power allocation variables can be optimized by solving the following problem,

$$(\mathcal{P}_2): \quad \max_{\eta_{mk}} \min_{k} SINR_k \quad \text{s. t. (C1) and (C4).} \qquad (14)$$

Here, we assume that maximizing $\min_k R_k$ and $\min_k SINR_k$ are equivalent since $R_k = \frac{\tau_c - \tau_p}{\tau_c} \log_2(1 + SINR_k)$. By applying a bisection method that has been extensively used in the context of CF massive MIMO [5], [6], [23], the power coefficients and the minimum desired rate can be achieved.

IV. Simulation Results

In our simulation of a cluster of LEO satellites, we consider a set of M SAPs serving a group of single-antenna ground UTs, with the channel conditions assumed static within a coherence time interval of τ_c samples. The Rician channel model is used, incorporating both LoS and NLoS components, with large-scale fading and losses represented by β_{mk}. Key simulation parameters include a satellite altitude of 550 km, an antenna factor of 20, a carrier frequency of 30 GHz, a shadowing standard deviation of 5 dB, a noise figure of 7 dB, noise power spectral density of -174 dBm/Hz, satellite's maximum power (P_m^{max}) of 15 dBW, satellite and UE antenna gains of 30 dB and 5 dB, respectively, pilot power (p_k) of 5 dBW, coherence intervals (τ_c, T_p) of 100 and 5 samples, and number of runs of 1e4. We also define $\sigma^2_{PF} = E\{|\delta^{\mathsf{P}}_{mk}|^2\} + E\{|\delta^{\mathsf{F}}_{mk}|^2\}$ as the summation of phase and frequency variances.

A. Results and Discussions

In Fig. 1, we can see the CDF of SINR among all users in the network. It can be easily understood that when $\sigma^2_{PF} \leq 10^{-2}$, interference from phase and frequency can be mitigated. However, by increasing the error, SINR decreases significantly. For Figs. 1 to 3, we assume a constant time synchronization error, which is 10% of its coherent gain ($\alpha_{mk} = 0.9$ for all m and k).

In Fig. 2, we compute the mean values for SAP association parameters, and it is interesting to note that when we have a high amount of synchronization errors, a smaller fraction of the available satellites can be achieved. This is because of

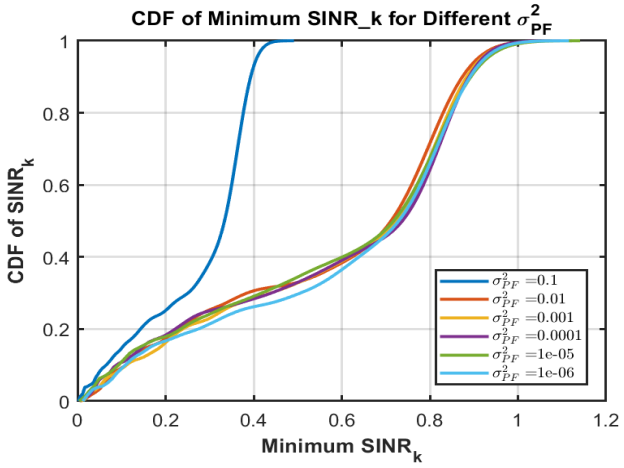

Fig. 1. CDF of Min $SINR_k$ for $K = 2$ and $M = 10$.

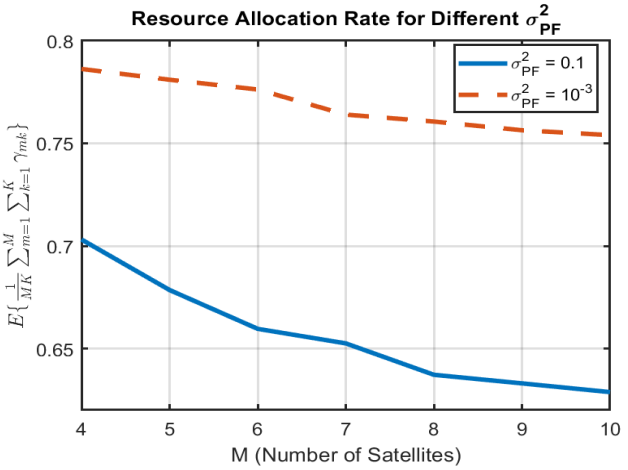

Fig. 2. SAP association expectation vs. number of SAPs for $K = 4$.

that the links where interference from phase and frequency synchronization errors will cause more degradation than their coherent gain, those links are being cut, resulting in fewer connections being used. With the same parameters, Fig. 3 indicates the achievable rate versus the number of satellites. It is interesting to see that for fewer synchronization errors, the user's rate increases much more than in the case where synchronization errors are high.

In Fig. 4, we observe the minimum user rate while keeping all parameters the same as in Fig. 3, except for fixing $\sigma^2_{PF} = 10^{-3}$ with two different values of α_{mk} ($\alpha_{mk} = 1$ and $\alpha_{mk} = 0.8$), where the first value indicates no time synchronization error. Unlike Fig. 3, the time synchronization effects are nearly identical for both cases. This similarity arises because time synchronization errors manifest as interference, and with power allocation being consistent, the minimum achievable rate shows a similar pattern. The key distinction lies in the phase and frequency synchronization errors, which do not contribute to interference but significantly affect computed beamforming due to their impact on the instantaneous channel.

Authorized licensed use limited to: Univ of Science and Tech Beijing. Downloaded on February 19,2025 at 04:30:09 UTC from IEEE Xplore. Restrictions apply.

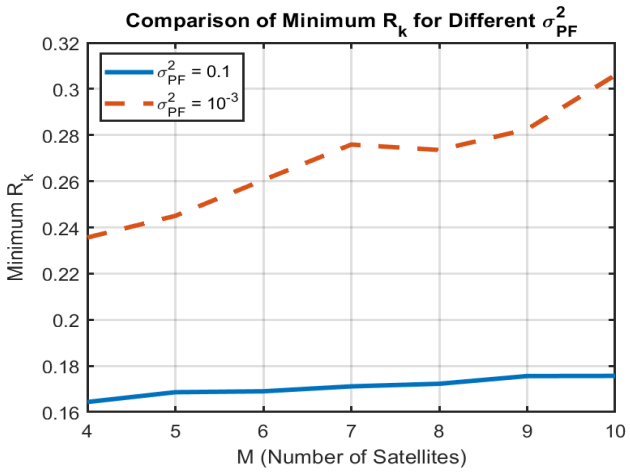

Fig. 3. Achievable rate vs. satellite count for two σ^2_{PF} values, $K = 4$.

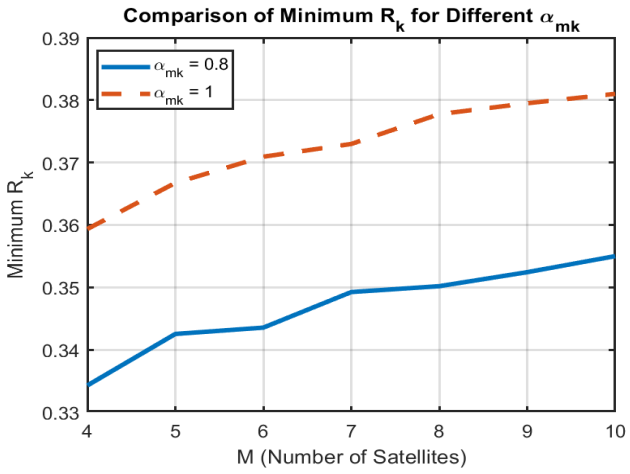

Fig. 4. Achievable rate vs. satellite count for two α_{mk} values, $K = 4$.

V. Conclusion

This study presents a pioneering approach by modeling the SINR in the context of CF mMIMO within UD-LEONs, taking into account synchronization errors in time, phase, and frequency. Our analyses unveil a critical insight: synchronization errors have a profound impact on the number of effective satellite links to users, underscoring the vital need to address these challenges. By incorporating advanced knowledge of synchronization error variances into resource allocation strategies, we not only enhance network efficiency and reliability but also pave the way for optimizing performance in future UD-LEONs. This study also highlights the requirement to develop novel channel estimation, innovative beamforming techniques, and advanced power allocation methods for future UD-LEONs to reduce synchronization errors and enhance system performance.

Acknowledgment

This work was supported by the Luxembourg National Research Fund (FNR), through the CORE Project (ARMMONY): Ground-based distributed beamforming harmonization for the integration of satellite and Terrestrial networks, under Grant FNR16352790.

References

[1] M. Y. Abdelsadek, G. Karabulut-Kurt, H. Yanikomeroglu, P. Hu, G. Lamontagne, and K. Ahmed, "Broadband Connectivity for Handheld Devices via LEO Satellites: Is Distributed Massive MIMO the Answer?," *IEEE Open J. Commun. Society*, vol. 4, 2023.

[2] V. N. Ha et al., "User-centric beam selection and precoding design for coordinated multiple-satellite systems", *arXiv:2403.08371*, 2024.

[3] J. C. M. Duncan et al., "Harnessing the Power of Swarm Satellite Networks with Wideband Distributed Beamforming," in *proc. 2023 PIMRC*, Canada, 2023.

[4] M. Y. Abdelsadek, G. K. Kurt, and H. Yanikomeroglu, "Distributed massive MIMO for LEO satellite networks," *IEEE Open Journal of the Communications Society*, vol. 3, pp. 2162–2177, 2022.

[5] J. Li, M. Liu, P. Zhu, D. Wang, and X. You, "Impacts of asynchronous reception on cell-free distributed massive MIMO systems," *IEEE Transactions on Vehicular Technology*, vol. 70, no. 10, 2021.

[6] J. Zheng, J. Zhang, J. Cheng, V. C. Leung, D. W. K. Ng, and B. Ai, "Asynchronous cell-free massive MIMO with rate-splitting," *IEEE Journal Sel. Areas in Commun.*, vol. 41, no. 5, 2023.

[7] J. Zhu, Y. Sun, and M. Peng, "Timing advance estimation in low earth orbit satellite networks," *IEEE Trans. Vehi. Tech.*, 2023.

[8] F. Kunzi and O. Montenbruck, "Precise onboard time synchronization for LEO satellites," *NAVIGATION: Journal of the Institute of Navigation*, vol. 69, no. 3, 2022.

[9] P. Chatterjee and J. A. Nanzer, "Effects of time alignment errors in coherent distributed radar," in *2018 IEEE Radar Conference (RadarConf18)*, April 2018, pp. 0727-0731.

[10] M. Rashid and J. A. Nanzer, "Frequency and phase synchronization in distributed antenna arrays based on consensus averaging and Kalman filtering," *IEEE Trans. Wireless Commun.*, vol. 22, no. 4, 2022.

[11] Y. Li, Q. Lin, Y. F. Liu, B. Ai, and Y. C. Wu, "Asynchronous activity detection for cell-free massive MIMO: From centralized to distributed algorithms," *IEEE Trans. Wireless Commun.*, vol. 22, no. 4, 2022.

[12] J. Zheng, Z. Zhao, J. Zhang, J. Cheng, and V. C. Leung, "Performance analysis of cell-free massive MIMO systems with asynchronous reception," in *2022 IEEE GC Wkshps*, December 2022.

[13] J. A. Nanzer, S. R. Mghabghab, S. M. Ellison, and A. Schlegel, "Distributed phased arrays: Challenges and recent advances," *IEEE Trans. Micro. Theory Tech.*, vol. 69, no. 11, 2021.

[14] S. R. Mghabghab, S. M. Ellison, and J. A. Nanzer, "Open-loop distributed beamforming using wireless phase and frequency synchronization," *IEEE Microwave and Wireless Components Letters*, vol. 32, no. 3, pp. 234–237, 2021.

[15] Y. Wan, J. Long, L. Liu, Z. Qian, and S. Zhong, "Downlink aware data scheduling with delay guarantees in resource-limited leo satellite networks," *Peer-to-Peer Networking and Applications*, vol. 14, 2021.

[16] W. Wang, T. Chen, R. Ding, G. Seco-Granados, L. You, and X. Gao, "Location-based timing advance estimation for 5G integrated LEO satellite communications," *IEEE Transactions on Vehicular Technology*, vol. 70, no. 6, pp. 6002-6017, 2021.

[17] J. M. Merlo, S. R. Mghabghab, and J. A. Nanzer, "Wireless picosecond time synchronization for distributed antenna arrays," *IEEE Transactions on Microwave Theory and Techniques*, vol. 71, no. 4,2022.

[18] Ö. Özdogan, E. Björnson, and J. Zhang, "Performance of cell-free massive MIMO with Rician fading and phase shifts," IEEE Transactions on Wireless Communications, vol. 18, no. 11, pp. 5299-5315, 2019.

[19] H. Nguyen-Kha, V. N. Ha, E. lagunas, S. Chatzinotas, and J. Grotz, "Joint Two-tier User Association and Resource Management for Integrated Satellite-Terrestrial Networks", *TechRxiv.23921631.v1*, 2023.

[20] V. N. Ha, J. C. M. Duncan, E. Lagunas, J. Querol, S. Chatzinotas. "Energy-Efficient Precoding and Feeder-Link-Beam Matching Design for Bent-Pipe SATCOM Systems", in *Proc. ICC 2023*.

[21] H. Nguyen-Kha, V. N. Ha, E. Lagunas, S. Chatzinotas, and J. Grotz, "Two-Tier User Association and Resource Allocation Design for Integrated Satellite-Terrestrial Networks," in proc. 2023 ICC Workshops, Rome, Italy, 2023.

[22] V. N. Ha, T. T. Nguyen, E. Lagunas, J. C. Merlano Duncan and S. Chatzinotas, "GEO Payload Power Minimization: Joint Precoding and Beam Hopping Design," in *proc. IEEE GLOBECOM 2022*.

[23] R. M. Zaeem, J. C. M. Duncan, W. A. Martins, V. N. Ha, S. Chatzinotas, and B. Ottersten, "Resource Allocation and User Scheduling Design for User-Centric Cell-Free Massive MIMO Systems," in *Proc. 2023 PIMRC*, 2023, pp. 1-6.

Authorized licensed use limited to: Univ of Science and Tech Beijing. Downloaded on February 19,2025 at 04:30:09 UTC from IEEE Xplore. Restrictions apply.